Hydraulics Laboratory

Civil Engineering Department

Katholieke Universiteit Leuven

MODELLING OF TURBULENCE DAMPING IN SEDIMENT-LADEN FLOW

Part 3

DRAG REDUCTION IN SEDIMENT-LADEN TURBULENT FLOW

Report No. HYD/ET/00/COSINUS5

December 2000

Erik A. TOORMAN

A contribution to the MAST III project COSINUS

MAST - III
Marine Science and Technology Programme

COSINUS

partially funded by the E.C., Directorate General XII under contract no. MAS3-CT97-0082.

DRAG REDUCTION IN SEDIMENT-LADEN TURBULENT FLOW

A contribution to Task A.1 of the COSINUS project

REPORT HYD/ET/00/COSINUS5

December 2000

by

Erik A. Toorman

Hydraulics Laboratory
K.U.Leuven

Acknowledgements

This work has been carried out within the framework of the MAST3 COSINUS project, funded in part by the European Commission, Directorate General XII for Science, Research & Development under contract no. MAS3-97-0082.

The authors post-doctoral position has been financed by the Flemish Fund for Scientific Research (FWO Vlaanderen).

Drag reduction in sediment-laden turbulent flow

1. INTRODUCTION

The major aim of the MAST3 COSINUS project is to provide new process models in a parameterized form, which can be implemented into currently used engineering models for sediment transport calculations. Task A has been investigating the modelling of sediment-turbulence interaction. An overview of this Task is given in (Toorman, 2000b, and Toorman *et al.*, 2000).

Drag reduction is the phenomenon where the resistance of a shear flow by friction along a solid surface is smaller than predicted by the traditional logarithmic velocity profile, which assumes a von Karman constant of 0.41. Drag reduction is furthermore characterised by a thickening of the viscous sublayer. Various mechanisms have been identified which can cause drag reduction. The most studied drag reduction phenomenon is that caused by (polymeric) additives (e.g. Lumley, 1969; Berman, 1978; Sellin *et al.*, 1982; Shenoy, 1988; Wilson, 1988). The drag reduction is explained by absorption of turbulent kinetic energy by vibrations of the polymeric chains.

Drag reduction occurs in fine-sediment-laden turbulent streams. Particularly in China, friction coefficients had to be modified significantly in order to predict the correct energy slope in rivers with high sediment concentrations. Apparent roughness values (Manning coefficients) smaller than for water over a glass plate had to be applied (Wang *et al.*, 1994).

Gust (1976) observed drag reduction in flume experiments with cohesive sediment suspensions. In analogy with drag reduction by polymeric additives, he hypothesised that vibrations in the floc structure could account for the energy absorption. New experiments with clay suspensions at higher concentrations have recently been published by Wang *et al.* (1998) and Li & Gust (2000). The latter found that the shear velocity can reduce by 70% at maximum.

Numerical experiments with the Prandtl mixing-length (PML) or the k-ε turbulence model, with implementation of damping functions, also predict drag reduction (e.g. Winterwerp, 1999; Toorman, 1999). This is observed in simple test cases were the flow rate is kept constant, and the sediment load varied. The model results show that the shear velocity decreases with increasing sediment load. However, the drag reduction in the simulations is smaller than observed in nature or laboratory experiments. Therefore, Winterwerp (1999) concluded that "the observed drag reduction cannot be explained by sediment-induced buoyancy effects alone". His numerical simulations predicted shear velocity reductions up to 3%, which is one order of magnitude smaller than in the experiments of Gust and Wang.

The Reynolds-stress model developed at LNH also yields a drag reduction for the so-called "Hanjalic" test case, i.e. u_* is 8% lower compared to the result of the uncoupled version where sediment does not influence hydrodynamics (Galland, 1996).

However, Toorman (2000b) argues that the models used have the damping functions implemented in an inconsistent way. The present report presents new model results obtained with the K.U.Leuven code FENST-2D, developed by the author, in which the damping functions have been implemented in a consistent way. The new model succeeds now in the prediction of the right magnitude of drag reduction.

2. MODEL DESCRIPTION

The present section summarizes the equations solved by the code FENST-2D and the closures used. Further details on the background of the model equations is found in (Toorman, 2000b).

2.1. Eddy viscosity and eddy diffusivity

The sediment transport models under consideration within the COSINUS project solve the Reynolds averaged Navier-Stokes (RANS) equations for the suspension hydrodynamics, where the Reynolds stresses have been replaced by the Boussinesq approximation, which introduces the (turbulent) eddy viscosity ν_t:

$$\rho\left(\frac{\partial U_i}{\partial t} + U_j\frac{\partial U_i}{\partial x_j}\right) = -\frac{\partial p}{\partial x_i} + \frac{\partial}{\partial x_j}\left(\rho\,(\nu+\nu_t)\left(\frac{\partial U_i}{\partial x_j}+\frac{\partial U_j}{\partial x_i}\right)\right) + f_i \qquad \textbf{(1)}$$

Similarly, the turbulent mixing in the sediment transport equation is replaced by the Boussinesq approximation, introducing the eddy diffusivity (or mixing coefficient) K_s:

$$\frac{\partial C}{\partial t} + U_j\frac{\partial C}{\partial x_j} = \frac{\partial}{\partial x_j}\left(K_s\frac{\partial C}{\partial x_j}\right) + \frac{\partial}{\partial z}\left(w_s C\right) \qquad \textbf{(2)}$$

where: C = sediment concentration (by mass), w_s = settling velocity. The eddy diffusivity is assumed to be proportional to the eddy viscosity:

$$\sigma_t = \frac{\nu_t}{K_s} \qquad \textbf{(3)}$$

where σ_t = the turbulent Schmidt number. Within the COSINUS project, the eddy viscosity (for the vertical mixing) is described either by the Prandtl mixing-length or by the k-ε turbulence model.

2.2. Prandtl mixing-length turbulence model

The Prandtl mixing length (PML) model is based on the hypothesis that the mixing length ℓ in simple, uni-directional near-wall shear flow is proportional to the distance (z) from the wall, i.e., in our case, the bottom:

$$\ell = \kappa z \qquad \textbf{(4)}$$

with κ = the von Karman coefficient (which has a value of 0.41 for isotropic turbulence, such as shear flow of homogeneous fluids far enough from the wall, known as the von Karman constant, which will be denoted here as κ_0). The eddy viscosity, according to the second hypothesis of Prandtl, reads:

$$\nu_t = \ell^2\left|\frac{\partial U}{\partial z}\right| \qquad \textbf{(5)}$$

We assume the flow to be horizontal only ($W = 0$) and take the x direction equal to the flow direction ($V = 0$). The x-momentum equation for fully-developed (i.e. steady) turbulent flow reads:

$$-\frac{\partial p}{\partial x} + \frac{\partial \tau}{\partial z} = 0 \qquad \textbf{(6)}$$

The pressure gradient is constant, i.e. $\partial p/\partial x = \mathrm{d}p/\mathrm{d}x$. The stress equilibrium over a certain rectangular domain between the wall and the distance z is obtained by integration between 0 and z:

$$\tau_0 = \rho u_*^2 = \tau(z) - z\frac{\mathrm{d}p}{\mathrm{d}x} = \rho\left(\nu + \nu_t\right)\frac{\partial U}{\partial z} - z\frac{\mathrm{d}p}{\mathrm{d}x} \qquad \textbf{(7)}$$

where: τ_0 = the wall shear stress, u_* = the shear velocity (by definition). When the wall distance is small enough, the pressure term can be neglected. Substitution of the eddy viscosity, eq.(5), and neglecting the kinematic viscosity (i.e. viscous stress << Reynolds stress, which is valid far enough from the bottom, e.g. for $z_+ = zu_*/\nu > 60$ when smooth) yields:

$$\frac{\partial U}{\partial z} = \frac{u_*}{\ell} = \frac{u_*}{\kappa z} \qquad \textbf{(8)}$$

Integration yields the velocity profile. When $\kappa = \kappa_0$ is constant, one finds the familiar logarithmic law:

$$u = \frac{u_*}{\kappa_0}\ln\left(z/z_0\right) \qquad \textbf{(9)}$$

where z_0 is a measure of the bottom roughness. This profile is also known as the "law of the wall". This result has been confirmed by numerous experiments. However, this is only correct for homogeneous fluids.

Expressing (7) at the water surface ($z = h$) where $\tau(h) = 0$ yields $\mathrm{d}p/\mathrm{d}x = \tau_0/h$. Hence, the vertical stress distribution in steady open-channel flow becomes (*cf.* eq.(7)):

$$\tau(z) = \nu_t\frac{\partial U}{\partial z} = \rho u_*^2\left(1 - z/h\right) \qquad \textbf{(10)}$$

Substitution of eq.(8) yields the eddy viscosity distribution in open-channel flow:

$$\nu_t = \kappa u_* z\left(1 - z/h\right) \qquad \textbf{(11)}$$

which is parabolic in the case of a constant κ. The corresponding mixing length distribution for open-channel flow is:

$$\ell = \sqrt{\frac{\nu_t}{\left|\frac{\partial U}{\partial z}\right|}} = \kappa z\sqrt{1 - z/h} \qquad \textbf{(12)}$$

2.3. Damping function definitions

The difference in turbulence between homogeneous and stratified fluids is expressed by semi-empirical correction factors, the damping functions. The basic definition for the damping functions, as employed throughout this report, is given by the ratio of stratified to homogeneous conditions (e.g. Munk & Anderson, 1948), i.e.:

$$\nu_t = \nu_0 F_t$$

$$K_s = K_0 F_s = \nu_0 \frac{F_s}{\sigma_0} \qquad \textbf{(13)}$$

F_t will be called the momentum damping function and F_s the mixing damping function. Hence, it follows that:

$$\sigma_t = \sigma_0 \frac{F_t}{F_s} \qquad \textbf{(14)}$$

$$\kappa = F_t \kappa_0 \qquad \textbf{(15)}$$

$$\ell = F_t \ell_0 \qquad \textbf{(16)}$$

where $\sigma_0 = \nu_0/K_0$ = the neutral turbulent Schmidt number (i.e. for $Rf = 0$), which has a generally accepted value of approximately 0.7, determined empirically (e.g. Turner, 1973).

Eq.(15) shows that F_t can also be considered as the correction factor for the von Karman constant. Experiments on sediment-laden turbulent flow already indicated that κ decreases with increasing concentration (e.g. Vanoni, 1946; Einstein & Chen, 1955). This hypothesis has been opposed by Coleman (1981), who believes that the decrease is only apparent and caused by the so called "wake effect" in the experimental flumes. The scientific community still seems to be divided over this issue. Recent numerical experiments with the research code FENST at the KUL support the original finding that κ indeed should decrease with increasing flux Richardson number Rf (Toorman, 1999).

2.4. Two-equation *k-ε* models

As the PML model cannot account for the history of turbulence and is only valid in simple shear flows, a more complex turbulence model is preferred in applied sediment transport modelling whenever possible. At present, the *k-ε* turbulence model seems to be the best compromise between computational cost and complexity, in particular with regard to coastal and estuarine engineering applications.

The eddy viscosity is defined in terms of turbulent kinetic energy k and energy dissipation rate ε:

$$\nu_t = f_\mu c_\mu \frac{k^2}{\varepsilon} \qquad \textbf{(17)}$$

with f_μ a low-Reynolds damping function. The *k*-ε model equations are:

$$\frac{\partial k}{\partial t} + U_i \frac{\partial k}{\partial x_j} = \frac{\partial}{\partial x_i}\left((\nu + \frac{\nu_t}{\sigma_k}) \frac{\partial k}{\partial x_i} \right) + P + G - \varepsilon \tag{18}$$

$$\frac{\partial \varepsilon}{\partial t} + U_i \frac{\partial \varepsilon}{\partial x_j} = \frac{\partial}{\partial x_i}\left((\nu + \frac{\nu_t}{\sigma_\varepsilon}) \frac{\partial \varepsilon}{\partial x_i} \right) + f_1 \frac{c_1}{T_t} \left(P + (1 - c_3) G \right) - f_2 c_2 \frac{\varepsilon}{T_t} \tag{19}$$

where the shear production of k is given by:

$$P = \nu_t \left(\frac{\partial U_i}{\partial x_j} + \frac{\partial U_j}{\partial x_i} \right) \frac{\partial U_i}{\partial x_j} \tag{20}$$

and the buoyancy damping by:

$$G = \frac{g}{\rho} \frac{\nu_t}{\sigma_t} \frac{\partial \rho}{\partial y} \tag{21}$$

The factor T_t is the turbulent time scale, which for fully-developed turbulent flow (i.e. high turbulent Reynolds number) is defined by:

$$T_t = \frac{k}{\varepsilon} \tag{22}$$

The factors f_1 and f_2 are used for the introduction of low-Reynolds effects. In the present study f_μ, f_1 and f_2 have the value 1, for high-Reynolds number conditions.

Damping by buoyancy effects is included in the k equation by the G term. It seems that the buoyancy term in the ε equation can be dropped, particularly in stable stratified shear flows (Rodi, 1980), i.e. $c_3 = 1$. Therefore, no buoyancy damping functions seem to be needed, except to describe the non-neutral Schmidt number in the buoyancy term of the k equation. However, also the boundary conditions for the k-ε model require the knowledge of the damping functions. This will be shown in the following sub-sections.

2.5. Richardson numbers

Stratification usually is characterized by a Richardson number, giving a ratio between buoyancy destruction and production of TKE. Several Richardson numbers have been defined in the literature.

The gradient Richardson number for the present 1DV case is defined as:

$$Ri = \frac{-g \frac{\partial \rho}{\partial z}}{\rho \left(\frac{\partial U}{\partial z} \right)^2} = \frac{-g \frac{\Delta \rho_s}{\rho_s} \frac{\partial C}{\partial z}}{\rho \left(\frac{\partial U}{\partial z} \right)^2} \tag{23}$$

Of more direct physical significance is the flux Richardson number *Rf*. The ***generalized*** flux Richardson number, as proposed by Ivey & Imberger (1991), is defined as:

$$Rf_g = -\frac{G}{M} = \frac{-G}{\varepsilon - G} \tag{24}$$

where: M = the mechanic production of TKE, i.e. including shear production, diffusion and inertia. Following this definition, one finds that the value of the general flux Richardson number at the free surface is always equal to 1.

Traditionally, the flux Richardson number is defined as the ratio of removal of energy by buoyancy to its production by shear only (Turner, 1973), i.e.:

$$Rf = -\frac{G}{P} = \frac{-g\,\overline{\rho' w'}}{\rho\,\overline{u' w'}\,\frac{\partial U}{\partial z}} = \frac{-\frac{g}{\sigma_s}\frac{\partial \rho}{\partial z}}{\rho\left(\frac{\partial U}{\partial z}\right)^2} = \frac{Ri}{\sigma_s} \tag{25}$$

where the Boussinesq approximation has been implemented to obtain the gradient form. The latter definition is only valid for steady state flows where inertia and diffusion of TKE are negligible (Toorman, 2000b).

2.6. Near-wall velocity profile for stratified shear flow

Having introduced various definitions, the derivation of the turbulent velocity profile in the near-wall layer can be revisited. Integration of eq.(8) for a non-constant κ yields the more general velocity profile:

$$u = \frac{u_*}{\kappa_0}\left(\ln\left(z/z_0\right) + \int_{z_0}^{z} \frac{1 - F_t}{z F_t}\,\mathrm{d}z\right) \tag{26}$$

and will deviate from the "law of the wall" when $F_t \neq 1$. It is easily shown that this corresponds to making the roughness parameter variable, i.e. eq.(9) can be replaced by:

$$u = \frac{u_*}{\kappa_0} \ln \frac{z}{\alpha(z) z_0} \tag{27}$$

where α = the friction correction factor. The corresponding velocity gradient is:

$$\frac{\partial U}{\partial z} = \frac{u_*}{\kappa_0 z}\left(1 + \frac{z}{\alpha}\frac{\partial \alpha}{\partial z}\right) \tag{28}$$

Hence:

$$F_t^{-1} = 1 + \frac{z}{\alpha}\frac{\partial \alpha}{\partial z} \tag{29}$$

Consequently, the effect of damping results in an apparent bottom roughness variation which changes with distance from the bed, i.e. the slope of the log-law is no longer constant.

2.7. Bottom boundary conditions

In the case of the standard high-Reynolds turbulence model, the boundary conditions for the k-ε equations are based on the 1D profiles of fully-developed turbulent flow over a flat surface (i.e. channel flow with $z_1 << h$). The dissipation rate in the wall node (ε_1) is obtained from the k conservation equation, eq.(18), assuming equilibrium between shear production, which is computed using the PML model approximation, and destruction of TKE:

$$\varepsilon_1 = P_1 + G_1 = \frac{u_*^3}{\kappa z_1}\left(1 - Rf\right) \qquad \textbf{(30)}$$

The turbulent kinetic energy in the near-wall node is then obtained from inserting ε_1 into the eddy viscosity definition, eq.(17), in which ν_t is approximated with the near-wall PML model, eq.(11) with $z/h << 1$:

$$k_1 = \frac{u_*^2}{\sqrt{c_\mu}}\sqrt{1 - Rf} \qquad \textbf{(31)}$$

Notice that traditional models do not consider the correction factor for stratification $(1 - Rf)^n$ (with $n = 1$ for ε_1 and $n = ½$ for k_1), which is only justifiable as long as $Rf << 1$.

In order to account for the presence of sediment in the low-Reynolds layer at the bottom, this layer is also included in the computational domain. The PML turbulence model is used within this layer. At the bottom the velocity is set equal to zero (non-slip condition). At the interface between the bottom layer and the turbulent layer, the boundary conditions for k, ε and velocity are imposed (i.e. Dirichlet conditions). The imposed velocity is obtained from the modified log-law, given by equation (27), and includes the friction modification factor.

2.8. Estimation of the shear velocity

The shear velocity u_* is a crucial parameter in the modelling of wall turbulence, especially when wall boundary conditions based on the PML theory are used. Most of the traditional k-ε models apply the law-of-the-wall at solid boundaries. The shear velocity u_* is required for the calculation of the near-wall boundary conditions for the variables velocity, TKE and dissipation rate.

Several methods can be applied to estimate the shear velocity. The various methods can be evaluated against a simple case of 1DV case of steady, fully-developed turbulent channel flow, driven by a constant pressure gradient $\mathrm{d}p/\mathrm{d}x$, for which the exact value of u_* is known (see above).

The shear velocity can be estimated from the velocity profile with eq.(8):

$$u_* = \kappa z \frac{\partial U}{\partial z} \qquad \textbf{(32)}$$

The result depends on the assumptions on κ and the methodology to determine the velocity gradient in the near-wall boundary node.

The von Karman coefficient κ usually is replaced by the constant κ_0 to determine u_*. As shown above, eq.(15), to be consistent, the von Karman constant should be corrected with the damping function F_t.

Traditionally, in most codes (including TELEMAC, the HR and DHI codes) the velocity gradient is obtained by elimination of u_* between the log-velocity profile, eq.(9), and its derivative, eq.(8), in which no damping is considered. This yields:

$$\frac{\partial U}{\partial z} = \frac{U}{z \ln(z/z_0)} \qquad \textbf{(33)}$$

When damping has to be considered, this is incorrect, which causes a serious problem. It can be overcome by introduction of a correction function f_u:

$$\frac{\partial U}{\partial z} = f_u \frac{U}{z \ln(z/z_0)} \qquad \textbf{(34)}$$

It can easily be shown with equations (27)-(29) that:

$$f_u^{-1} = F_t \left(1 - \frac{\ln \alpha}{\ln(z/z_0)} \right) \qquad \textbf{(35)}$$

The convergence behaviour of this method is somewhat slower, but the potential problem of error generation and propagation is avoided. However, the function f_u itself is a problem, because it contains the poorly known apparent roughness modification factor α (see Section 4).

A safer method is the estimation of the velocity gradient using one or the other interpolation function for the velocity. As the difference between the velocities is small, a differentiation error may be generated which may cause numerical problems (this happens in the KUL code FENST with the specific fortran compiler used if no truncation is applied). This may be a big disadvantage of this method. The convergence behaviour, however, is good.

An intermediate solution may be to consider a logarithmic interpolation function of the form $U = a \ln z - b$. The corresponding velocity gradient in node "1" can then be found as:

$$\frac{\partial U_1}{\partial z} = \frac{U_1 - U_2}{z_1 \ln(z_1/z_2)} \qquad \textbf{(36)}$$

where "2" refers to a neighbouring node. This approximation is good as long as the value of the damping function does not change too much between the two nodes. This is only the case when far enough from saturation.

The previous methods result in computed shear velocities which deviate slightly from the theoretical value in the case of steady-state 1DV flow. In the case of the k-ε model, the best value for the shear velocity is obtained from the stress balance over a volume with thickness dx and height z from the wall:

$$u_* = \sqrt{\left(\nu + c_\mu \frac{k^2}{\varepsilon} \right) \frac{\partial U}{\partial z} - \frac{z}{\rho} \frac{\partial p}{\partial x}} \qquad \textbf{(37)}$$

Again the velocity gradient is required. Evaluation for channel flow shows that with the traditional boundary conditions for k and ε, this value of u_* may overpredict the true shear velocity considerably when the pressure gradient term is neglected. The convergence behaviour is much better than with the previous method.

Including the pressure gradient term has the additional advantage that one can take the first node "far" away from the bed (i.e. up to $z_+ = z u_*/\nu \approx 1000$). This will allow much more

accurate performance on the coarse vertical grids used for real application.

In practice, the value of u_* affects the value of the variable only at the near-wall boundary node. Fortunately, except near the bottom boundary, the velocity gradients over the water column are not affected because of the stress balance, and therefore, neither are the turbulence profiles (k, ε and ν_t). Only the velocity profile is shifted over a certain Δu, which is the error between the estimated and the real shear velocity. The error Δu can become significant in when approaching saturation, as will be demonstrated below.

3. NUMERICAL EXPERIMENTS

3.1. Test case definition

A numerical experiment has been carried out with the PML model to illustrate the problem with the traditional models and how the consistent model yields very different results compared to the traditional method. The steady state 1DV test case consists of the fully-developed turbulent open-channel flow driven by a constant pressure gradient, such that the shear velocity is known[1] from:

$$u_* = \sqrt{\frac{h}{\rho}\frac{\mathrm{d}p}{\mathrm{d}z}} \tag{1}$$

For the present case, the parameters are: channel depth h = 16 m, horizontal pressure gradient $\mathrm{d}p/\mathrm{d}x$ = 0.04 Pa/m. The corresponding shear velocity is 0.008 m/s. The settling velocity w_s = 1 mm/s.

3.2. Results

First, the traditional boundary treatment approach, where the damping function is not taken into account for the calculation of the shear velocity, is applied. The error on the estimated shear velocity grows to 70% at saturation. This implies that the bed shear stress is overestimated by a factor 3 !

In the next step, the damping function is taken into account at this stage, but not in the velocity boundary condition in the near-bottom node (i.e. $\alpha = 1$). The solution is improved with regard to the estimation of the shear velocity. When approaching saturation, the error still increases, but remains below 10%.

Variation of the value of α shows that this does not affect the estimation of u_* significantly (except when the velocity gradient over the bottom layer becomes very large), neither does it change the concentration profile. With this knowledge, the numerical data from the previous method can be used to calculate α by integrating equation (29), using trapezoidal numerical integration. The corrected velocity profile can then be drawn, as $-(u_*/\kappa_0)\ln(\alpha)$ is the difference Δu over which the velocity profile has to be shifted. Applying the corresponding value of α in the code to the velocity boundary condition, yields a velocity profile, slightly higher than the theoretically reconstructed one, which can be explained by the error on the calculation of α by numerical integration over the bottom layer, which is inaccurate due to the large gradients and the few (i.e. three) integration points.

[1] A study at constant flow rate is less evident because the shear velocity is not known a priori.

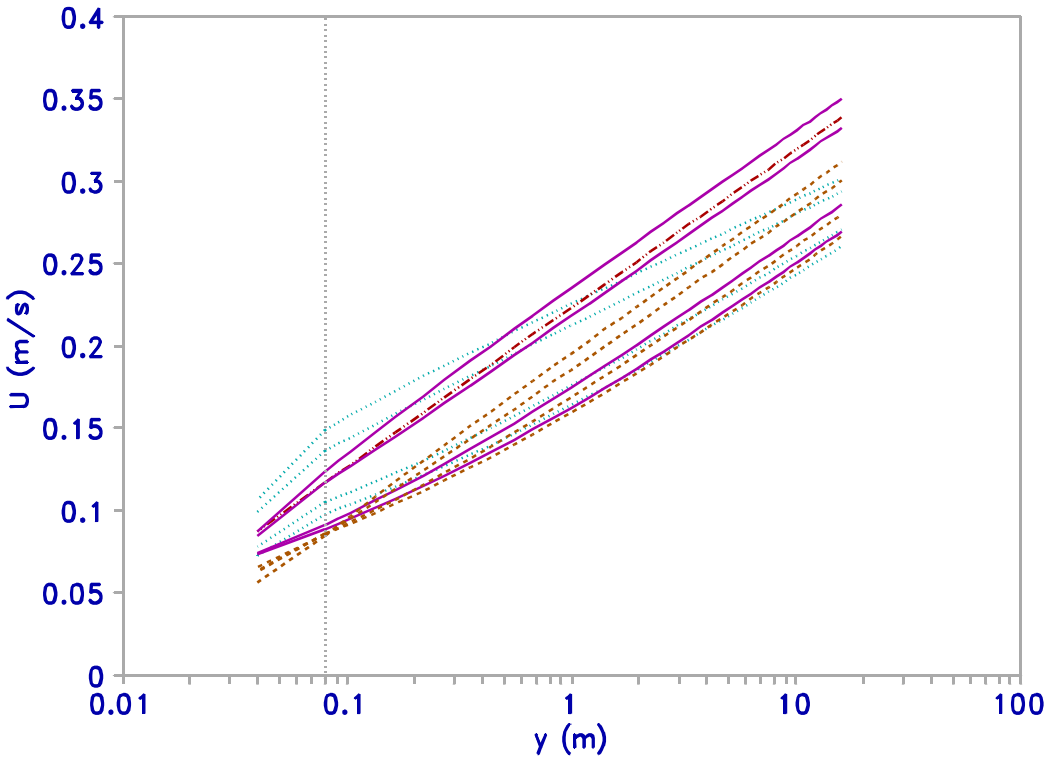

Figure 1: Velocity profiles ($dp/dx = 0.04$ Pa/m, $h = 16$ m) obtained with the PML model for 4 different sediment loads (increasing from bottom to top). Dotted line = inconsistent traditional method; dashed line = consistent u_* calculation; full line = fully consistent solution obtained with theoretical friction correction of previous; centered line = numerical solution of fully consistent approach with friction correction from previous.

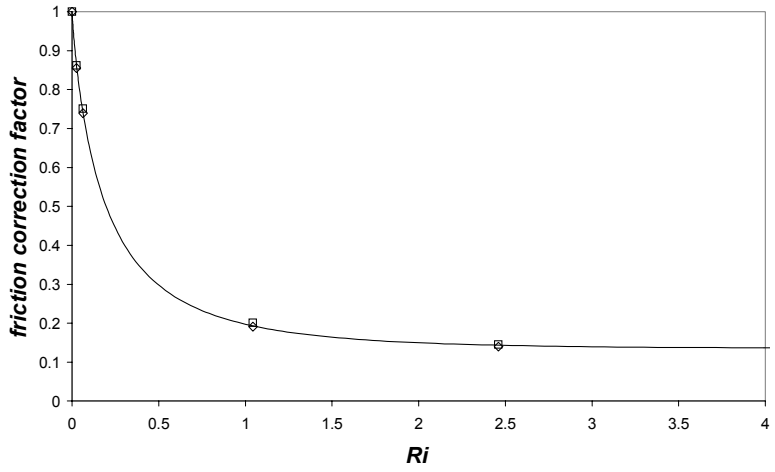

Figure 2: Variation of the friction correction coefficient as a function of Ri for the above test case ($w_s/u_* = 1/8$). Symbols = numerical data (◇ from integration and □ from difference in simulated u respectively), line = equation (39).

The following empirical formula is found for the friction correction factor α (figure 2):

$$\alpha = \exp\left[-\left(1 + (1 + a\, w_s/u_*)\right)\left(1 - \exp(-bRi^{n})\right)\right] \qquad \textbf{(39)}$$

with parameter values: $a = 7.7$, $b = 1/0.6$ and $n = 0.85$. These parameter values may deviate from the "correct" values, as it is the result of integration over the bottom layer alone. Nevertheless, the shift Δu of the velocity profile can then be computed from the numerical results, which is equal to $-(u_*/\kappa_0)\ln(\alpha)$, resulting in friction correction factors close to those obtained by integration (figure 2).

3.3. Implications

By implementing the damping factors in a consistent way the correct shear velocity is well approximated. In the previous example the true shear velocity has been held constant by imposing a constant energy slope (i.e. a constant horizontal pressure gradient). A similar numerical experiment where the flow rate is held constant can be carried out as well. This has been done in a previous study (Toorman, 1999), however with the traditional inconsistent implementation and another value of the parameter c_3 (0 instead of 1) in the ε equation. The conclusion in the above study that the inconsistent method overpredicts the bed shear stress, can also be applied in the reverse way to the case with constant flow rate. It implies that the bed shear stress decreases with increasing sediment load down to 30% (at saturation) of the value for clear water at the same flow rate. Interestingly, this corresponds exactly to the maximal drag reduction measured in the flume experiments by Li & Gust (2000).

The previous study (Toorman, 1999), where also the case was studied where the sediment load has been held constant and the shear velocity varied, shows that the flow rate initially decreases with u_*, reaches a minimum and then increases again as a consequence of drag reduction. From these results it has been concluded that for a constant flow rate, the flow may evolve to a non-saturated condition or a condition close to saturation, depending on the history. From the intercomparison exercise within Task E of the COSINUS project (Violeau, 2000), it has been noticed that the final result (either saturated or non-saturated), can be influenced by the numerical techniques implemented in the code, i.e. the explicit and implicit numerical diffusion.

3.4. Physical interpretation

The previous sections provide a modelling framework for the simulation of drag reduction in fine-grained sediment-laden turbulent shear flows, which proves to allow estimations of the right order of magnitude of observed drag reduction. This does not explain what actually happens.

Apparently, the friction correction seems to imply a decrease of the effective roughness, since its value is smaller than 1 for stratified flow conditions. When considering the velocity profile, defined by eq.(27), one has to bear in mind the general form of the roughness parameter:

$$z_0 = \frac{\nu}{Eu_*} + \frac{k_s}{B} \qquad \textbf{(40)}$$

where: E (= ±9) = the smooth-wall roughness parameter, and B (= 30) the rough wall roughness parameter. The physical roughness height k_s does not change. The effective suspension viscosity increases due to particle-particle and fluid-particle interactions, which can explain in part the

thickening of the sublayer. But the non-dimensional profile can never get above the smooth-wall profile. In order to obtain roughnesses lower than "smooth", as observed in field conditions and simulated by the model as shown above, the roughness parameters E and B should increase with Ri.

It seems strange that for the same energy input (same u_*) the transport rate of the flow increases more than expected due to drag reduction. At the basis of the phenomenon lies the damping of turbulence by buoyancy effects. Turbulence is induced due to flow instabilities by friction along the bottom. Due to the buoyancy damping less energy is lost by turbulent dissipation and more will be available for transport.

The condition of saturation seems to correspond to a condition of optimal energetic conditions for particle transport by suspensions. During sub-saturation conditions more energy is dissipated by turbulence and less is available for transport.

Once over-saturated, the amount in excess will remain in the bottom layer, contributing to the thickening of the sublayer, and thus reducing the flow depth where the optimal conditions apply. More energy will be lost in the bottom layer and less will be available for transport.

It still remains unclear what happens in the near-bottom layer, which includes the transition layer and the viscous sublayer. These layers also have some transport capacity. The transition layer certainly has suspended transport, because turbulence is still very important (the turbulence production is maximal at a wall distance which corresponds to the section of the laminar and fully turbulent velocity profiles, respectively $u_+ = z_+$ and $u_+ = \ln(z/\alpha z_0)/\kappa$, in non-dimensional form; Toorman, 2000a). For larger particles interactions between particles may contribute to a great extend to enhance turbulence and help explain the occurrence of sheet flow. In this case an apparent increase of drag is expected.

3.5. Comparison with data

The data of Cellino (1998) have been analysed. The reduction of the Reynolds stress of the thick near-bottom layer cannot be explained by the concentration effect, neither by Bagnolds grain shear stress, which has been derived for low-Reynolds flow conditions. In other words, the grain shear stress under turbulent conditions is much higher.

The viscous stress of the suspension is estimated using the Krieger equation:

$$\nu = \nu_f \left(1 - \varphi/\varphi_{\max}\right)^{-2.5\varphi_{\max}} \qquad \textbf{(41)}$$

The viscous stress cannot account entirely for the reduction of the Reynolds stress. Considering the fact that this semi-empirical law is only valid for laminar flow, its underestimation is no surprise. Additional fraction losses due to turbulent particle-interaction is expected to explain.

The grain shear stress τ_G, introduced by Bagnold (1954) is described by:

$$\tau_G = \alpha \rho_s \left(\lambda d \frac{\mathrm{d}U}{\mathrm{d}z}\right)^2 + \beta f(\lambda) \mu_f \frac{\mathrm{d}U}{\mathrm{d}z} \qquad \textbf{(42)}$$

The first term represents the so-called inertia region and the second the viscous region. Various empirical relationships $f(\lambda)$ and different values for α and β have been proposed (Bagnold, 1954; Savage & McKeown, 1983; Mih, 1993). The data of Bagnold and Savage *et al.* (1983, 1984) have been obtained for relatively large particles (1-2 mm) at high concentrations in a Couette flow at relatively low Reynolds numbers. Applied to the data of Cellino, one finds grain shear stresses much too small to explain the observations. Cellino's data suggest that the contribution in turbulent flows is much higher (up to 5 times the viscous stress).

4. CONCLUSIONS

Considerable drag reduction is observed in certain rivers carrying high suspended cohesive sediment loads. Drag reduction is also measured in laboratory flume experiments with clay suspensions. Thus far, sediment transport models did not succeed in simulating these conditions, to the same extend.

Reconstruction of the basic mixing-length turbulence model with consistent implementation of buoyancy damping functions provides a semi-empirical theoretical framework which explains the occurrence of drag reduction and the decrease of the von Karman coefficient in sediment-laden turbulent shear flows. The new theory has been implemented in the research code FENST-2D at the K.U.Leuven, both into the PML and the k-ε turbulence models. Application of the model to various scenarios of steady open-channel flow where the sediment load or the shear velocity is varied shows that the expected amount of drag reduction is predicted by the model, relative to experiments by Li & Gust (2000).

A friction correction factor, which can be related to the momentum damping function by an integral relation, has been introduced and a methodology to determine its functional relationship is presented. This factor is found to be a function of the ratio w_s/u_* and of the Richardson number.

The present model is not suitable to deal with the condition of super-saturation, where the bottom layer outside the fully-developed turbulent layer thickens. This may be important for the correct prediction of sediment transport around flow reversal at slack tides. Future work will investigate possibilities to extend the model's abilities to low-Reynolds modelling. Some preliminary attempts are described in (Toorman, 2000a and 2000b).

REFERENCES

Bagnold, R.A. (1954). Experiments on a gravity-free dispersion of large solid spheres in a Newtonian fluid under shear. *Proc. Roy. Soc. London A (Math. & Phys. Sci.)*, Vol.225:49-70.

Berman, N.S. (1978). Drag reduction by polymers. *Ann. Rev. Fluid Mech.*, 10:47-64.

Cellino, M. (1998). Experimental study of suspension flow in open-channels. PhD thesis, Dept. de Genie Civil, Ecole Polytechnique Fédérale de Lausanne.

Coleman, N.L. (1981). Velocity profiles with suspended sediment. *J. Hydr. Res.* **19**(3):211-229.

Einstein, H.A. & N. Chien (1955). Effects of heavy sediment concentration near the bed on velocity and sediment distribution. *M.R.D. Sediment Series*, No.8, Missouri River Div., US Army Corps of Engineers.

Galland, J.-C. (1996). Transport de sédiments en suspension et turbulence. Report HE-42/96/007/A, L.N.H., Chatou.

Gust, G. (1976). Observations on turbulent drag reduction in a dilute suspension of clay particles. *J. Fluid Mech.*, 75(1):29-47.

Hanjalic, K., M. Ivanovic, V. Vujovic & V. Milisic (1982). Buoyancy effects and mutual interaction of suspended particles and velocity field in turbulent shear flows. In: *Structure of Turbulence in Heat and Mass Transfer*, Proc. ICMH, Hemisphere Editions.

Ivey, G.N. & J. Imberger (1991). On the nature of turbulence in a stratified fluid. Part I: The energetics of mixing. *J. Physical Oceanography*, 21:650-658.

Li, M.Z. & G. Gust (2000). Boundary layer dynamics and drag reduction in flows of high cohesive sediment suspensions. *Sedimentology*, 47:71-86.

Lumley, J.L. (1969). Drag reduction by additives. *Ann. Rev. Fluid Mech.*, 1:367-384.

Mih, W.C. (1993). An empirical shear stress equation for general solid-fluid mixture flow. *Int. J. Multiphase flow*, 19(4):683-690.

Munk, W.H. & E.A. Anderson (1948). Notes on a theory of the thermocline. *J. Marine Research*, 3(1):276-295.

Rodi, W. (1980). *Turbulence models and their application in hydraulics.* IAHR State-of-the-art Paper, IAHR, Delft.

Savage, S.B. & S. McKeown (1983). Shear stresses developed during rapid shear of concentrated suspensions of large spherical particles between concentric cylinders. *J. Fluid Mechanics*, 127:453-472.

Savage, S.B. & M. Sayed (1984). Stresses developed by dry cohesionless granular materials sheared in an annular shear cell. *J. Fluid Mechanics*, 142:391-430.

Sellin, R.H.J., J.W. Hoyt & O. Scrivener (1982). The effect of drag-reducing additives on fluid flows and their industrial applications. Part 1: Basic aspects. *J. Hydraulic Research*, 20(1):29-68.

Sellin, R.H.J., J.W. Hoyt, J. Pollert & O. Scrivener (1982). The effect of drag-reducing additives on fluid flows and their industrial applications. Part 1: Basic aspects. *J. Hydraulic Research*, 20(3):235-292.

Shenoy, A.V. (1988). Turbulent flow velocity profiles in drag-reducing fluids. *Encyclopedia of Fluid Mechanics*, 7:479-503, Gulf Publ. Co., Houston, TX.

Toorman, E.A. (1999). Numerical simulation of turbulence damping in sediment-laden flow. Part 1. The "Siltman" test case and the concept of "saturation". Report HYD/ET/99.2, Hydraulics Laboratory, K.U.Leuven.

Toorman, E.A. (2000a). Analysis of near-wall turbulent shear flows. Report HYD/ET/00/ COSINUS2, Hydraulics Laboratory, K.U.Leuven.

Toorman, E.A. (2000b). Parameterisation of turbulence damping in sediment-laden flow. Report HYD/ET/00/COSINUS3, Hydraulics Laboratory, K.U.Leuven.

Toorman, E.A., A.W. Bruens, C. Kranenburg & J.C. Winterwerp (2000). Interaction of suspended cohesive sediment and turbulence. *6th Int. Conf. on Nearshore and Estuarine Cohesive Sediment Transport Processes* (Delft, September 2000), submitted.

Turner, J.S. (1973). *Buoyancy Effects in Fluids*, Cambridge University Press, Cambridge.

Vanoni, V.A. (1946). Transportation of suspended sediment by water. *Trans. ASCE*, 111:67-133.

Violeau, D. *et al.* (2000). 1DV test case (subtask E.2). Intercomparison of the preliminary results. *COSINUS Task E Interim Report* (January 2000), LNHE, Chatou.

Violeau, D., C. Le Normant & C. Cheviet (2000). Siltman 1DV case. Comparison of several numerical models. MAST-3 COSINUS European Project, Report HP-72/2000/042/A, LNHE, EDF, Chatou, France, 20 pp.

Wang, Z.Y. & P. Larsen (1994). Turbulent structure of water and clay suspensions with bed load. *J. Hydraulic Eng.*, Vol.120(5)577-600, ASCE.

Wang, Z.Y., Larsen, P., Nestmann, F. & Dittrich, A. (1998). Resistance and drag reduction of flows of clay suspensions. *J. Hydr. Eng.*, Vol.124(1):41-49.

Wilson, K.C. (1988). Mechanisms of drag reduction in turbulent non-Newtonian pipe flow. *Encyclopedia of Fluid Mechanics*, 7:505-523, Gulf Publ. Co., Houston, TX.

Winterwerp, J.C. (1999). On the dynamics of high-concentrated mud suspensions. PhD thesis, T.U. Delft.